Received: 4 January 2024 | Revised: 21 June 2024 | Accepted: 1 July 2024

DOI: 10.1002/cac2.12590

CANCER COMMUNICATIONS Open Access

LETTER TO THE JOURNAL

Dual inhibition of sirtuins 1 and 2: reprogramming metabolic energy dynamics in chronic myeloid leukemia as an immunogenic anticancer strategy

Chronic myeloid leukemia (CML) is a lethal hematopoietic malignancy with a global incidence primarily attributed to the *breakpoint cluster region-Abelson* (BCR-ABL1) fusion oncogene in over 95% of cases. The introduction of tyrosine kinase inhibitors (TKIs) has revolutionized CML management; however, a subset of patients encounters challenges such as resistance and relapse, hindering the achievement of complete remission. Overcoming these challenges in CML also requires addressing persistent leukemia stem cells (LSCs) with inherent resistance mechanisms. Key regulators of LSC metabolism, proliferation, and survival, as well as genetic and epigenetic alterations, provide potential targets [1].

In this study, leveraging in silico analysis (methods and descriptions of other assays are in the Supplementary file) of LSCs from CML patients at diagnosis, we demonstrated enrichment in pathways predominantly associated with proliferation, oxidative phosphorylation (OXPHOS), and metabolism, concurrently with a decrease in immune response pathways (Figure 1A). Similarly, genes negatively impacting proliferation in CML cell lines, when depleted by CRISPR, were enriched in processes related to OXPHOS, metabolism, and proliferation, mirroring the enrichment observed in LSCs (Figure 1B) [2].

Sirtuins (SIRTs) are nicotinamide adenine dinucleotide $(NAD)^+$-dependent histone deacetylases. SIRT1 and SIRT2 modulate key signaling proteins impacting metabolism, survival, and stress response [3]. Overexpression of SIRT1 and SIRT2 was observed in various cancers, including leukemia (Supplementary Figure S1A) [4, 5]. However, our analysis of CML patients revealed variability in the expression levels of SIRT1 and SIRT2 across datasets (Supplementary Figure S1B). Given the relatively small sample sizes, we recognized the limitations of relying solely on single gene expression data, as it may not fully capture the functional relevance of SIRT1/2 in CML. In response to this limitation, we expanded our analysis to identify broader gene expression patterns associated with SIRT1/2. Specifically, we identified a CML-related network comprising 180 co-regulated transcriptional targets associated with SIRT1/2 enriched in genes relevant to leukemia (Figure 1C, Supplementary Figure S1C-E). To quantify their collective impact, we consolidated the expression of all transcripts in the SIRT1/2 regulon into a unified score, referred to as the SIRT1-2 regulon score. This score effectively discriminated between healthy hematopoietic stem cells and LSCs from CML patients at diagnosis (Figure 1D), indicating the collective impact of SIRT1 and SIRT2 on the disease.

Given the complementary roles of SIRT1 and 2 in regulating metabolic and survival pathways and their potential to compensate for each other's loss of function [3], we postulated that exploiting metabolic vulnerabilities in LSCs through dual targeting of SIRT1 and SIRT2 activities could profoundly influence CML cell survival. We first verified the constitutive SIRT1 and SIRT2 expression levels in myeloid cell lines and showed that their genetic and pharmacological inhibition, including with the compound Si-711 [6], reduced proliferation and total HDAC activities in CML cells (Supplementary Figures S1F, S2-S3). Si-711 has favorable pharmacokinetics and pharmacodynamics parameters and demonstrated superior activities compared to other reference SIRT inhibitors (Supplementary Tables S1-S3,

Abbreviations: ATP, adenosine triphosphate; BCR-ABL1, *breakpoint cluster region-Abelson*; CD, cluster of differentiation; CML, chronic myeloid leukemia; CRISPR, clustered regularly interspaced short palindromic repeats; DAMPs, damage-associated molecular patterns; ECAR, extracellular acidification rate; HMGB, high mobility group box; ICD, immunogenic cell death; LSC, leukemia stem cell; MLKL, mixed lineage kinase domain-like pseudokinase; MYC, myelocytomatosis; NAD, nicotinamide adenine dinucleotide; OCR, oxygen consumption rate; OXPHOS, oxidative phosphorylation; P_PBMCs, proliferating PBMCs; PARP, poly (ADP-ribose) polymerase; PBMCs, peripheral blood mononuclear cells; RIPK, receptor-interacting serine/threonine-protein kinase; SIRT, sirtuin; TKI, tyrosine kinase inhibitor.

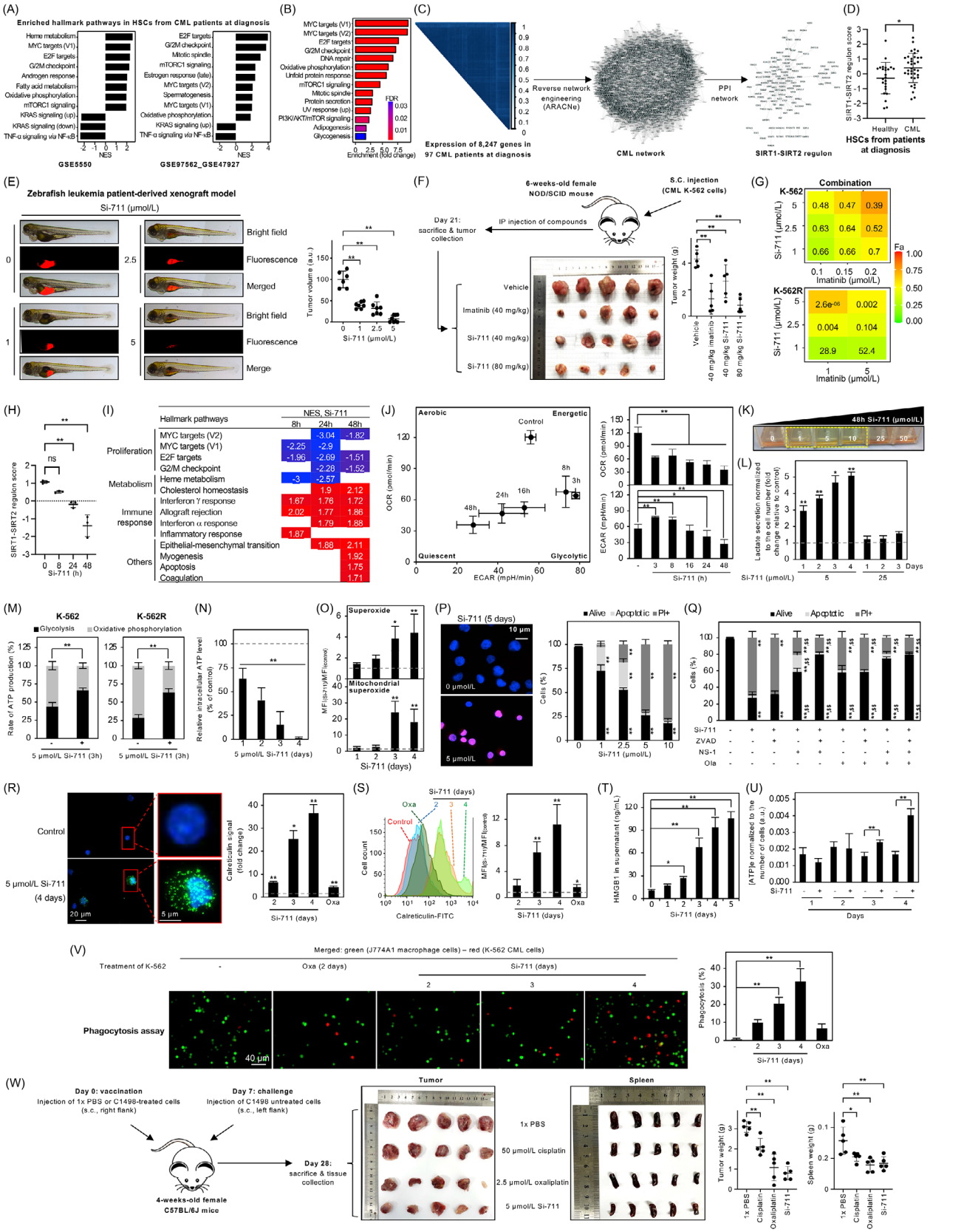

FIGURE 1 Simultaneous inhibition of SIRT1 and SIRT2 rewires cell metabolism, leading to growth inhibition and immunogenic cell death in CML, and synergizes with imatinib. (A) NES of all significant (adjusted *P*-value < 0.05) hallmark pathways altered in CD34$^+$ HSCs from CML patients compared to their healthy counterparts determined by GSEA performed in GSE5550 (left panel) and combined GSE97562_GSE47927 (right panel) data sets. (B) Enriched hallmark pathways based on the knockout (CRISPR) of genes with negative median effects on proliferation across a CML cell line panel from Project Achilles data. Pathways with significant enrichment (FDR adjusted *P* < 0.05)

are highlighted. (C) SIRT1-2 regulon construction overview. The correlation plot (left panel) depicts gene expression profiles of CML patients at diagnosis ($n = 97$), showing high consistency in expression patterns. A disease-specific network (middle panel) was constructed to extract the SIRT1-2 regulon, including SIRT1 and SIRT2 nodes with their first-degree connections. A PPI network was built to explore known interactions within the regulon (right panel). (D) Scatter plot comparing SIRT1-2 regulon scores in healthy ($n = 24$) and CML ($n = 36$) patients, with each data point representing an individual sample. (E) Patient-derived leukemia cells with a BCR-ABL rearrangement were treated at the indicated concentrations of Si-711 for 48h, fluorescently labeled, and then injected into the zebrafish yolk sac. Three days post-injection, phase contrast and fluorescent (red) pictures of fishes were acquired (left panel: representative images from a total of $n = 5$ to 10 fishes per condition are shown), and the fluorescence intensity was quantified (right panel). (F) Pictures of tumors excised from K-562-xenograft mice ($n = 5$ per group) treated by IP injection as indicated in the figure and their corresponding weight. (G) Si-711 synergistically kills CML cells in combination with imatinib. Left panels: heatmap representing the Fa for each combination with increasing concentrations of Si-711 and imatinib after 72h of incubation. Numbers on the heatmap represent the combination index for each condition of treatment. (H) Scatter plot depicting dynamic changes in SIRT1-SIRT2 regulon scores based on transcriptomic data from K-562 cells treated with 5 μmol/L Si-711. (I) Heatmap highlighting the changes in NES for hallmark pathways based on GSEA of transcriptomic data from K-562 cells treated with 5 μmol/L Si-711 for the indicated time points versus control cells. Significant positive NES in red indicates upregulation or the activation of associated pathways, whereas significant negative NES in blue indicates significant downregulation or suppression of associated pathways. The corresponding significant GSEA-enrichment plots are presented in Supplementary Figure S12B-D. (J) Evolution of the metabolic profile of K-562 cells treated with 5 μmol/L Si-711 for up to 48h evaluated by OCR and ECAR measurements to assess mitochondrial respiration and glycolysis, respectively. Left panel: energy phenotype. Right panels: quantifications of OCR and ECAR parameters. (K) K-562 cells were treated with increasing concentrations of Si-711 for two days, and culture flasks were photographed to document the color of the cell culture media. Rectangles with dashed yellow lines indicate the range of concentrations of Si-711 leading to enhanced medium acidification compared to the control. (L) Lactate secretion measurements in K-562 cell supernatant. (M) Quantification of ATP production rate from oxidative phosphorylation and glycolysis. (N) Intracellular ATP levels in K-562 cells. (O) Superoxide and mitochondrial superoxide levels in K-562 cells treated with 5 μmol/L Si-711 for up to 4 days expressed as the MFI ratio between treated and control cells reported to isotype controls. (P) Nuclear morphology analysis in K-562 cells treated with increasing concentrations of Si-711. Left panel: merged UV-microscopy pictures representative of at least three independent experiments of cells stained with Hoechst (blue) and PI (red) after 5 days of incubation in the absence (0 μmol/L; all cells are displaying intact chromatin and proper nuclear morphology corresponding to alive cells) or presence of 5 μmol/L Si-711 (most cells have a round nucleus with PI uptake indicating necrotic cells). Right panel: quantification of apoptotic, PI-positive, and alive cell populations. (Q) Quantification of apoptotic, PI-positive, and alive cell populations from nuclear morphology analyses on K-562 cells treated with the chemical inhibitors of PARP1 (1 μmol/L ola), caspases (50 μmol/L ZVAD), and RIPK1 (60 μmol/L NS-1) and incubated in the presence or absence of 5 μmol/L Si-711 for 5 days. (R-U) Increased levels of ICD-associated release of DAMPs from Si-711-treated CML K-562 cells. Oxaliplatin served as a positive control for DAMPs release and ICD induction. (R, S) Analysis of calreticulin exposure by UV-microscopy and flow cytometry, respectively, in K-562 cells treated with 5 μmol/L Si-711 for up to 4 days and 40 μmol/L oxaliplatin for 2 days. (R) Left panel: merged UV-microscopy pictures representative of at least three independent experiments of cells stained with Hoechst (blue) and immunostained for calreticulin (green) at 40× magnification. Right panel: quantification of the corresponding calreticulin signal. (S) Left panel: representative histogram of at least three independent experiments. Right panel: quantification of the corresponding calreticulin signal expressed as the MFI ratio between treated and control cells reported to isotype controls. (T, U) Kinetic analyses of HMGB1 and ATP release, respectively, in the cell culture supernatant of K-562 cells treated with 5 μmol/L Si-71l. (V) Macrophage-mediated phagocytosis of Si-711-treated CML cells. K-562 cells stained in red were treated for the indicated time with 5 μmol/L Si-711 and co-incubated with J774A1 macrophages stained in green. Left panel: merged UV-microscopy pictures of the red and green channels, representative of at least three independent experiments. Right panel: quantification of the corresponding percentage of phagocytosis. (W) Pictures and weight of tumors and spleens excised from mice ($n = 5$ per group) vaccinated or not (1× PBS) with dying C1498 myeloid leukemia cells following the treatment with cisplatin (50 μmol/L), oxaliplatin (2.5 μmol/L) or Si-711 (5 μmol/L) and challenged by alive C1498 cells as indicated in the figure. L, N, O, R, S The dashed line represents the level in control cells. All graphs represent the mean ± SD of at least three independent experiments. *P*-values were calculated by one-way ANOVA with Dunnett's multiple comparison tests (unpaired for E, F, H, J, P, T, V, W; paired for L, N, R, S) or Šidák's multiple comparison tests (Q), and unpaired two-tailed t-tests (D, M, O, U). * and ** indicate $P < 0.05$ and $P < 0.01$, respectively, versus control. $^{\$\$}$ indicates $P < 0.01$ *versus* Si-711-treated cells. Abbreviations: [ATP]e, extracellular ATP; A.u., arbitrary units; ANOVA, analysis of variance; ARACNe, algorithm to reconstruct accurate cellular networks; ATP, adenosine triphosphate; CD, cluster of differentiation; CML, chronic myeloid leukemia; CRISPR, clustered regularly interspaced short palindromic repeats; DAMPs, damage-associated molecular patterns; ECAR: extracellular acidification rate; Fa, fractional inhibition; FDR, false discovery rate; FITC, fluorescein isothiocyanate; GSEA, gene set enrichment analysis; HMGB1, high-mobility group box 1; HSC, hematopoietic stem cell; ICR, immunogenic cell death; IP, intraperitoneal; MFI, mean fluorescence intensity; mTOR, mammalian target of rapamycin; mTORC1, mTOR complex 1; MYC, myelocytomatosis, NES, normalized enrichment score; NF-κB, nuclear factor-κB; NOD/SCID, nonobese diabetic/severe combined immunodeficiency; NS-1, necrostatin-1; OCR, oxygen consumption rate; Ola, olaparib; Oxa, oxaliplatin; PARP, poly (ADP-ribose) polymerase; PBS, phosphate-buffered saline; PI, propidium iodide; PI3K, phosphoinositide 3-kinase; PPI, protein-protein interaction network; RIPK, receptor-interacting serine/threonine-protein kinase; s.c., subcutaneous; SD, standard deviation; SIRT, sirtuin; TNF, tumor necrosis factor; ZVAD, Z-VAD(OMe)-FMK.

Supplementary Figures S4-S5). We demonstrated that Si-711 induced robust cytostatic effects concomitant with G1 arrest in various myeloid leukemia cells, including both TKI-sensitive and -resistant models, exhibiting a good selectivity for cancer cells (selectivity factor ranging from 3 to 18) compared to normal cells (Supplementary Table S3, Supplementary Figures S6-S7, S8A). Inhibiting SIRT1/2 activities reduced the viability of primary CML cells from patients *ex vivo* and significantly inhibited cell growth in leukemia patient-derived xenograft zebrafish and CML cell xenograft mouse models without signs of toxicity (Figure 1E-F, Supplementary Figure S9, Supplementary Tables S4-S5). Additionally, Si-711 treatment significantly reduced the aldehyde dehydrogenase-positive subpopulation of CML cells (Supplementary Figure S10), a marker of stemness, indicating its potential efficacy against LSCs. Moreover, Si-711 strongly synergized with imatinib, the first-line therapy against CML, in both imatinib-sensitive and -resistant CML cell lines (Figure 1G, Supplementary Figure S11), potentially overcoming resistance mechanisms observed in some CML cases.

RNA-sequencing of Si-711-treated K-562 CML cells for up to 48 h was conducted to investigate mechanistic aspects. We validated the SIRT1-2 score established from patient data, showing that Si-711 significantly reduced this score in a time-dependent manner (Pearson test, $r = 0.92$, $P < 0.001$; Figure 1H, Supplementary Figure S12A). Differentially expressed genes were analyzed, revealing a downregulation of genes involved in proliferation, enriched in those regulated by key transcription factors such as MYC, JUN, and E2F4, which have extensive connections to the SIRT1/2 regulon, and an upregulation of genes associated with the immune response and cell death mechanisms (Figure 1I, Supplementary Figures S12B-H, S13). Metabolic reaction enrichment analysis revealed that, at 24 h, Si-711 induced significant metabolic alterations in CML cells, including upregulation of glycolysis and downregulation of nucleotide metabolism and mitochondrial respiratory complexes (Supplementary Figure S12I-Q). *In cellulo* investigations revealed that SIRT1/2 inhibition induced critical metabolic alterations in CML, leading to a decrease in oxygen consumption rate (OCR), a transient increase in extracellular acidification rate (ECAR), and ultimately, a reduction in overall metabolic activity (Figure 1J, Supplementary Figure S14A-G). As an adaptive response to the inhibition of OCR, Si-711 enhanced glycolysis, leading to increased extracellular acidification, lactate release, and a shift of CML cells towards predominant glycolytic-dependent ATP production, deviating from their initial reliance on OXPHOS-dependent ATP (Figure 1K-M, Supplementary Figures S8B, S14H-K, S15A), a characteristic of LSCs and therapy-resistant cells [7]. Ultimately, these metabolic alterations resulted in a progressive depletion in total ATP content, significant changes in the NAD^+/NADH ratio, and morphological alterations in mitochondria, including onion-like swirling cores surrounded by swollen spaces, accompanied by a less condensed and disorganized cristae structure (Figure 1N, Supplementary Figures S8C, S14L, S15B-C, S16-S18). Furthermore, Si-711 treatment increased mitochondrial superoxide levels, suggesting the induction of oxidative stress (Figure 1O, Supplementary Figure S19). Upon prolonged exposure, the resulting energetic collapse directed the fate of most myeloid leukemia models toward necrosis-like cell death at concentrations ranging from 5-10 μmol/L, selectively targeting cancer cells with selectivity factors ranging from 10 to 105 (Figure 1P, Supplementary Figures S8D, S20-S22, Supplementary Table S6). This non-canonical cell death is distinct from traditional anti-CML therapies, holding promise for overcoming canonical apoptotic resistance mechanisms [8]. The inhibition of SIRT1/2 induced a caspase/RIPK3-independent but RIPK1/MLKL/PARP1-dependent necrosis (Figure 1Q, Supplementary Figures S23-S26). This necrosis led to a progressive depletion of endoplasmic reticulum calcium storage, causing its accumulation in mitochondria associated with the opening of the mitochondrial permeability transition pore (Supplementary Figures S24, S27-S30). SIRT1/2 inhibition with Si-711 induced immunologic regulated necrosis in CML cells, significantly promoting the release of damage-associated molecular patterns (DAMPs), including calreticulin, high mobility group box 1 (HMGB1), and ATP (Figure 1R-U, Supplementary Figure S31A-E). This can potentially trigger immunogenic cell death (ICD) and enhance the anticancer immune response [9]. Notably, Si-711 treatment boosted phagocytosis (Figure 1V, Supplementary Figure S31F), indicating a potential increase in immune response. We conducted an in vivo vaccination assay, which is considered the gold standard to validate the induction of ICD and assess therapeutic potential [10]. Upon tumor challenge, mice vaccinated with Si-711-treated cells exhibited a significant reduction in tumor volume, tumor weight, and splenomegaly (Figure 1W, Supplementary Figures S32-S33). Importantly, Si-711's effects in inducing ICD were found to be comparable to the known ICD inducer oxaliplatin.

In conclusion, we propose SIRT1/2 inhibition, particularly with Si-711, as a promising and innovative therapeutic strategy for CML. The dual targeting of SIRT1 and SIRT2 could eradicate LSCs through metabolic reprogramming and induction of immunogenic necrosis-like cell death. This comprehensive approach holds the potential for addressing challenges such as resistance and relapse in CML, providing new avenues for improved patient outcomes.

AUTHOR CONTRIBUTIONS

Michael Schnekenburger performed in vitro/*in cellulo* experiments; Sruthi Reddy Gajulapalli, Ridhika Rajora, and Jin-Young Lee performed in vivo experiments; Hyoung Jin Kang provided patient samples; Aloran Mazumder and Haeun Yang performed additional in vitro experiments; Anne Lorant performed, analyzed, and interpreted bioinformatic data and statistical analyses; Christo Christov interpreted and analyzed histological sections; Michael Schnekenburger and Marc Diederich conceived and designed the project. Michael Schnekenburger, Anne Lorant, and Marc Diederich wrote/edited the manuscript; Bernard Pirotte synthesized the inhibitor; Marc Diederich supervised the project. All authors have read and approved the manuscript. Marc Diederich is responsible for all aspects of this work, including descriptions, illustrations, and data accuracy.

ACKNOWLEDGMENTS

Not applicable

CONFLICT OF INTEREST STATEMENT

The authors declare no conflict of interest.

FUNDING INFORMATION

LBMCC: "Recherche Cancer et Sang" foundation, the "Recherches Scientifiques Luxembourg", the "Een Häerz fir kriibskrank Kanner", the Action LIONS "Vaincre le Cancer" and Télévie Luxembourg. SNU: National Research Foundation (NRF) (Grant Number 370C-20220063); MEST of Korea for Tumor Microenvironment Global Core Research Center (GCRC) (Grant Number 2011-0030001); Brain Korea (BK21) PLUS program and Creative-Pioneering Researchers Program at Seoul National University (Funding number: 370C-20160062). Sruthi Reddy Gajulapalli and Ridhika Rajora were supported by grants for the "Graduate Scholarship for Excellent Foreign Students" program.

DATA AVAILABILITY STATEMENT

The raw RNA-seq data generated during the current study are available in GEO under the accession number GSE248894 (the link to the dataset will be released after manuscript acceptance).

The data generated during this study are included in this published article and its supplementary information files.

The datasets analyzed during the current study are available from the corresponding author upon reasonable request.

ETHICS APPROVAL AND CONSENT TO PARTICIPATE

All animal experiments were conducted following the guidelines set by the "Korean Food and Drug Administration". Protocols were reviewed and approved by the "Institutional Animal Care and Use Committee of Seoul National University" (approval numbers: SNU-201006-2 [NOD/SCID xenograft model], SNU-210518-10-2 [vaccination assay], SNU-191218-5-1 [zebrafish]).

For human leukemia samples, the Institutional Review Board of Seoul National University Hospital reviewed and approved the study protocol and exempted the study from the obligation to obtain informed consent. This study was performed following the World Medical Association's **Declaration of Helsinki**.

PBMCs and P_PBMCs were used with the approval of the National Research Ethics Committee of Luxembourg. PBMCs were isolated from blood obtained from the Red Cross (Luxembourg, Luxembourg) under the authorization LBMCC-2019-0002: "Assessment of toxicity of new drugs or drug combinations in preclinical development in nonproliferating peripheral blood mononuclear cells (systemic acute toxicity)". P_PBMCs were generated from blood obtained from the Red Cross under the authorization LBMCC- 2019-0001: "Assessment of differential toxicity of new drugs or drug combinations in preclinical development in *ex-vivo* proliferating peripheral blood mononuclear cells vs. proliferating cancer cells."

The obtention of umbilical cord blood samples for the isolation of $CD34^+$ cells was approved by the board of directors of the Bohler clinic (Hôpitaux Robert Schuman, Luxembourg, Luxembourg). Tissues were obtained anonymously with the written informed consent of parents with the approval of the National Research Ethics Committee of Luxembourg.

Michael Schnekenburger[1]
Anne Lorant[1]
Sruthi Reddy Gajulapalli[2]
Ridhika Rajora[2]
Jin-Young Lee[2]
Aloran Mazumder[2]
Haeun Yang[2]
Christo Christov[3]
Hyoung Jin Kang[4]
Bernard Pirotte[5]
Marc Diederich[2]

[1]*Laboratoire de Biologie Moléculaire et Cellulaire du Cancer, Luxembourg, Luxembourg*
[2]*Research Institute of Pharmaceutical Sciences & Natural Products Research Institute, College of Pharmacy, Seoul National University, Seoul, Republic of Korea*

[3]*Faculté de Médecine, Université de Lorraine, Vandœuvre-lès-Nancy, France*
[4]*Department of Pediatrics, Seoul National University College of Medicine, Seoul National University Cancer Research Institute, Seoul National University Children's Hospital, Seoul, Republic of Korea*
[5]*Laboratory of Medicinal Chemistry, Center for Interdisciplinary Research on Medicines (CIRM), University of Liège, Liège, Belgium*

Correspondence
Marc Diederich, Department of Pharmacy, College of Pharmacy, Seoul National University, Building 21 Room 218, 1 Gwanak-ro, Gwanak-gu, Seoul, 08826, Republic of Korea.
Email: marcdiederich@snu.ac.kr

Present address
Jin-Young Lee, Department of Biological Sciences, Keimyung University, Daegu 42601, Republic of Korea
Aloran Mazumder, Aging and Cancer Immuno-Oncology, Sanford Burnham Prebys Medical Discovery Institute, La Jolla, 92037, California, USA

Michael Schnekenburger and Anne Lorant are equal contributors to this work and designated as co-first authors

ORCID

Marc Diederich https://orcid.org/0000-0003-0115-4725

REFERENCES

1. Koschmieder S, Vetrie D. Epigenetic dysregulation in chronic myeloid leukaemia: A myriad of mechanisms and therapeutic options. Semin Cancer Biol. 2018;51:180–197.
2. Kuntz EM, Baquero P, Michie AM, Dunn K, Tardito S, Holyoake TL, et al. Targeting mitochondrial oxidative phosphorylation eradicates therapy-resistant chronic myeloid leukemia stem cells. Nat Med. 2017;23(10):1234–1240.
3. Wu QJ, Zhang TN, Chen HH, Yu XF, Lv JL, Liu YY, et al. The sirtuin family in health and disease. Signal Transduct Target Ther. 2022;7(1):402.
4. Carafa V, Altucci L, Nebbioso A. Dual Tumor Suppressor and Tumor Promoter Action of Sirtuins in Determining Malignant Phenotype. Front Pharmacol. 2019;10:38.
5. Chen G, Huang P, Hu C. The role of SIRT2 in cancer: A novel therapeutic target. Int J Cancer. 2020;147(12):3297–3304.
6. Schnekenburger M, Goffin E, Lee JY, Jang JY, Mazumder A, Ji S, et al. Discovery and Characterization of R/S-N-3-Cyanophenyl-N'-(6-tert-butoxycarbonylamino-3,4-dihydro-2,2-dimethyl-2H-1- benzopyran-4-yl)urea, a New Histone Deacetylase Class III Inhibitor Exerting Antiproliferative Activity against Cancer Cell Lines. J Med Chem. 2017;60(11):4714–4733.
7. de Beauchamp L, Himonas E, Helgason GV. Mitochondrial metabolism as a potential therapeutic target in myeloid leukaemia. Leukemia. 2022;36(1):1–12.
8. Diepstraten ST, Anderson MA, Czabotar PE, Lessene G, Strasser A, Kelly GL. The manipulation of apoptosis for cancer therapy using BH3-mimetic drugs. Nat Rev Cancer. 2022;22(1):45–64.
9. Kroemer G, Galassi C, Zitvogel L, Galluzzi L. Immunogenic cell stress and death. Nat Immunol. 2022;23(4):487–500.
10. Fucikova J, Kepp O, Kasikova L, Petroni G, Yamazaki T, Liu P, et al. Detection of immunogenic cell death and its relevance for cancer therapy. Cell Death Dis. 2020;11(11):1013.

SUPPORTING INFORMATION

Additional supporting information can be found online in the Supporting Information section at the end of this article.